

**ARTICLE**

# Grid-Connected Control Strategy of VSG under Complex Grid Voltage Conditions

**Bin Zhang and Yanjun Jin\***

School of Automation &amp; Electrical Engineering, Lanzhou Jiaotong University, Lanzhou, China

\*Corresponding Author: Yanjun Jin. Email: [jjj19893175170@163.com](mailto:jjj19893175170@163.com)

Received: 09 July 2021 Accepted: 24 September 2021

**ABSTRACT**

Under complex grid conditions, the grid voltage usually has an imbalance, low order harmonics, and a small of DC bias. When the grid voltage contains low order harmonics and a small amount of DC bias component, the inverter's output current cannot meet the grid connection requirements, and there is a three-phase current imbalance in the control strategy of common VSG under unbalanced voltage. A theoretical analysis of non-ideal power grids is carried out, and a VSG control strategy under complex operating conditions is proposed. Firstly, the third-order generalized integrator (TOGI) is used to eliminate the influence of the DC component of grid voltage. An improved delay signal cancellation (DSC) method is proposed to control the balance current and power fluctuation under unbalanced voltage based on the method of common VSG positive and negative sequence separation, It also eliminates the harmonic of command current. Then, the improved quasi proportional resonant controller (QPR) cascaded PI is used to suppress the harmonic current further so that the harmonic content of grid-connected current can meet the grid-connected requirements and achieve the three-phase current balance. Finally, the proposed strategy is verified by simulation under the control objectives of the current balance, active power, and reactive power constant.

**KEYWORDS**

Complicated condition; harmonic elimination; VSG control; DC component; quasi-proportional resonance; sequence current control

## 1 Introduction

With the rapid development of new energy and high level accesses to the distribution network, the damping and inertia of the power system also decrease accordingly. The common grid-connected inverter has defects in providing frequency and voltage support for the power grid. Therefore, it cannot meet the power system's frequency, and voltage regulation performance with a large number of distributed generation penetration. As a result, the stability problem of power system is becoming increasingly serious. Therefore, when the distributed generation is connected to the grid, it should also support the grid voltage and frequency actively. In recent years, the application of virtual synchronous generator (VSG) grid-connected inverter control in the field of new energy has attracted attention [1–4]. The synchronous generator port voltage characteristics, provide the corresponding inertia and damping support for the grid when the distributed generation is connected to the grid [5–9]. Auxiliary



inertia and additional power are introduced into VSG, which reduces the difference between VSG and SG and improves transient stability [10,11].

However, most of the research on VSG is based on the condition of three-phase voltage balance. However, in the actual operation of the power system, the grid voltage is usually affected by various factors, resulting in three-phase voltage imbalance, DC bias component and harmonic content. When the grid voltage is unbalanced, including DC component and harmonic content, VSG will have grid-connected current distortion and output active power and reactive power oscillation just like an ordinary inverter. In reference [12], it is proposed to reshape the voltage admittance of the power grid and use the voltage feed-forward of the power grid to suppress the current harmonics. Still, there is no research on the unbalanced power grid and the DC component. In reference [13], the VSG control strategy is mainly studied from the perspective of limiting over-current. In reference [14], the strategy of suppressing harmonic resonance by series resistance or parallel resistance of filter capacitor is proposed. Wan et al. considered in-depth research on the power grid voltage imbalance, but did not further discuss that the power grid voltage contains harmonics and small DC components [15]. In the two-phase static coordinate system, the positive sequence and negative sequence of grid voltage are decomposed to realize the coordinated control of power and current and improve the operation performance of the system [16]. When the power grid voltage contains harmonics and a small DC component, its control strategy will fail. Hu et al. considered virtual impedance based on positive and negative sequence control of output current, which can limit the fault current when the grid voltage drop [17]. The suppression of power grid harmonic and the elimination of DC components are not discussed. In reference [18], the improved PR controller is applied to the harmonic suppression of PMSM. Xiao et al. used a second-order generalized integrator to separate the positive and negative sequence of voltage and current [19]. When the power grid voltage is unbalanced, it is verified according to different control objectives, but the control strategy will fail when it contains DC component. In reference [20], an active damping control strategy is proposed based on the voltage and current's positive and negative sequence components. The current harmonic is suppressed, but this strategy fails when the grid voltage contains a DC component. Shi et al. proposes that in case of power grid failure, PR current control algorithm is used to limit the power grid current and provide reactive power to the power grid [21]. The phase angle feedback tracking synchronization strategy is adopted to improve the transient performance of the switching process. This strategy will not achieve the control goal when the power grid contains a DC component.

The control strategies proposed in the above literature do not consider the unbalanced grid voltage, harmonic and DC components. Considering the above situation, this paper takes the three-phase balance of output current and constant power as the control objectives when the grid voltage of VSG grid-connected inverter is unbalanced and contains harmonics and a small DC components. It proposes a pre-third-order generalized integrator to eliminate DC components. The improved DSC achieves the current command balance and harmonic elimination based on the VSG control strategy under common voltage imbalance [22]. The improved quasi proportional resonance (QPR) controller cascaded with PI controls the command current. Control strategy when the grid voltage is unbalanced and contains harmonics and DC components simultaneously, or under any of the non-ideal conditions, the control goal can be achieved without selecting the control strategy according to the type of non-ideal grid voltage. Finally, the correctness of the proposed strategy is verified by Simulink simulation in the case of unbalanced grid voltage, harmonic, and DC components.

## 2 Analysis of Voltage Composition and Power Fluctuation of the Power Grid

Assuming that the grid voltage is not ideal, that is, including DC offset component, three-phase voltage imbalance, and each harmonic component, the three-phase grid voltage can be expressed as

$$e_k = e_{0k} + \sum_{h=1}^{\infty} [e_h^+ \cos(h\omega t + \theta_{hk}^+) + e_h^- \cos(h\omega t + \theta_{hk}^-)] \quad (1)$$

where:  $k = a, b, v$ ;  $e_{0k}$  is DC component;  $e_h^+$  ( $e_h^-$ ) is the positive (negative) sequence voltage amplitude;  $h$  is the number of harmonics;  $\theta_{hk}^+$  ( $\theta_{hk}^-$ ) is the positive (negative) sequence phase of  $k$ -phase voltage.

The third-order generalized integrator can eliminate the DC component of the non-ideal grid voltage in the three-phase static coordinate system. After eliminating the DC component, the non-ideal grid voltage can be expressed as

$$e_k = \sum_{h=1}^{\infty} [e_h^+ \cos(h\omega t + \theta_{hk}^+) + e_h^- \cos(h\omega t + \theta_{hk}^-)] \quad (2)$$

It can be seen from reference [23] that after the grid voltage is transformed through 3 s/2r coordinate, the  $h$ -th harmonic will be transformed into  $h + 1$  or  $h - 1$  harmonic.

When the grid voltage is unbalanced, the expressions of instantaneous active power and reactive power are as follows:

$$\begin{cases} P(t) = P_0 + P_{c2} \cos(2\omega t) + P_{s2} \sin(2\omega t) \\ Q(t) = Q_0 + Q_{c2} \cos(2\omega t) + Q_{s2} \sin(2\omega t) \end{cases} \quad (3)$$

where:

$$\begin{cases} P_0 = 1.5(e_d^+ i_d^+ + e_q^+ i_q^+ + e_d^- i_d^- + e_q^- i_q^-) \\ P_{c2} = 1.5(e_d^+ i_d^- + e_q^+ i_q^- + e_d^- i_d^+ + e_q^- i_q^+) \\ P_{s2} = 1.5(e_q^- i_d^+ - e_d^- i_q^+ - e_q^+ i_d^- + e_d^+ i_q^-), \end{cases} \begin{cases} Q_0 = 1.5(e_q^+ i_d^+ - e_d^+ i_q^- + e_q^- i_d^- - e_d^- i_q^+) \\ Q_{c2} = 1.5(e_q^+ i_d^- - e_d^+ i_q^- + e_q^- i_d^+ - e_d^- i_q^+) \\ Q_{s2} = 1.5(e_q^- i_d^+ - e_d^- i_q^+ + e_q^+ i_d^- - e_d^+ i_q^-) \end{cases}$$

where  $e_{dq}$  is the component of grid voltage in the dq coordinate system, the superscript “-” represents negative sequence component, and the superscript “+” represents the positive sequence component.

## 3 VSG Control Strategy

The essence of fractional VSG is to simulate the output characteristics of a synchronous generator, so that the grid-connected inverter can have the characteristics and advantages of a synchronous generator. The overall block diagram of the main circuit of fractional VSG is shown in Fig. 1. In Fig. 1,  $u_{dc}$  is DC side voltage,  $Z_s$  is inverter side impedance, C is filter capacitor, and  $Z_g$  is grid side impedance.  $i_a$ ,  $i_b$  and  $i_c$  are the output current of the inverter,  $u_a$ ,  $u_b$  and  $u_c$  are the output voltage of the inverter, and  $P^*$  and  $Q^*$  are the initial set values of the output active and reactive power.

During grid-connected operation, the VSG power frequency and excitation control loop transmits power to the grid according to the initial set of active and reactive power. To calculate the reference phase and frequency, the active power loop of VSG simulates the primary frequency modulation, damping and inertia of SG. As the power system frequency must be within the allowable range, to meet this requirement, the VSG power frequency control loop must analyze the influence of frequency deviation on VSG. As a virtual synchronous motor, the frequency can be adjusted as long as the mechanical torque is controlled. In terms of power, the frequency can also be adjusted by controlling the output power and the given power, as shown in Eq. (4); Then the phase angle of the inverter side

output voltage is adjusted according to the mechanical equation of the synchronous generator  $\theta$ .

$$T_m = \frac{P^*}{\omega} - k_f(f - f_0) \quad (4)$$

where  $f$ ,  $f_0$  and  $k_f$  are the voltage frequency of inverter terminal, the reference frequency of the power grid and the frequency deviation adjustment coefficient, respectively.

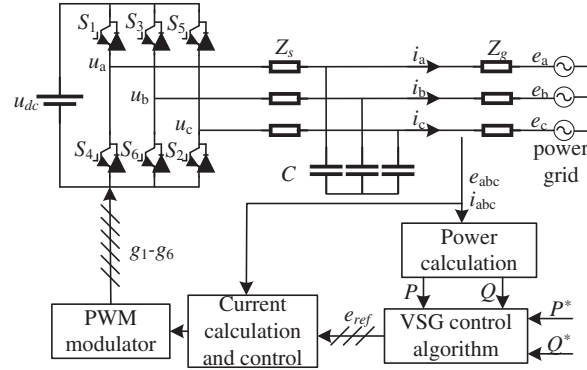


**Figure 1:** Overall block diagram of VSG main circuit

VSG excitation control loop adjusts the output reactive power and voltage amplitude of grid-connected inverter, as shown in Eq. (5); The voltage amplitude  $e$  obtained by the excitation control loop and the phase angle obtained by the power frequency control loop are used  $\theta$ . The synthetic reference voltage  $u_{ref}$  is shown in Eq. (6), while the VSG control block diagram is shown in Fig. 2.

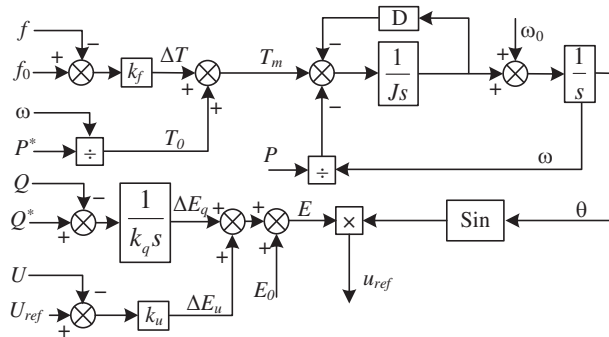


**Figure 2:** Block diagram of VSG control

$$E = E_0 + \frac{1}{k_q s} (Q^* - Q) + k_u (U_{ref} - U) \quad (5)$$

where:  $k_q$  is the adjustment coefficient of reactive power deviation,  $Q^*$  is the initial given value of inverter reactive power,  $Q$  is the output reactive power value of inverter,  $k_u$  is the adjustment coefficient of voltage amplitude deviation,  $U_{ref}$  is the initial given effective value of terminal voltage,  $U$  is the output voltage value of inverter,  $E_0$  is the voltage reference value.

$$u_{ref} = \begin{bmatrix} E \sin(\theta) \\ E \sin(\theta - 2\pi/3) \\ E \sin(\theta + 2\pi/3) \end{bmatrix} \quad (6)$$

## 4 VSG Control Strategy under Complex Conditions

### 4.1 Reference Current Calculation

According to Eq. (3), current balance or constant power control can be realized under unbalanced grid voltage by controlling the values of positive and negative sequence currents. The calculation of the current reference value is the core part of the whole control, which is the key to realize current balance and power oscillation suppression. Therefore, the calculation method of the current reference value is introduced below.

According to Fig. 1, the relationship between the output voltage and current of inverter is established without considering the effect of the capacitor, as shown in Eq. (7):

$$u_{abc}^* = -Ri_{abc} - L \frac{di_{abc}}{dt} + e_{abc} \quad (7)$$

where  $L$  and  $R$  are the total inductance and the total resistance from the inverter to the grid, respectively.

The output voltage  $u_{abc}$  of the inverter side is decomposed into dq by the d-axis orientation of the grid voltage, and the relationship between voltage and current in the dq coordinate system is as follows:

$$\begin{bmatrix} u_d \\ u_q \end{bmatrix} = \begin{bmatrix} e_d \\ e_q \end{bmatrix} + \begin{bmatrix} Lp + R & -\omega L \\ \omega L & Lp + R \end{bmatrix} \begin{bmatrix} i_d \\ i_q \end{bmatrix} \quad (8)$$

If Eq. (8) is transformed into complex frequency domain calculation, the expression of current reference instruction is as follows:

$$\begin{aligned} \begin{bmatrix} I_d^* \\ I_q^* \end{bmatrix} &= \begin{bmatrix} Lp + R & -\omega L \\ \omega L & Lp + R \end{bmatrix}^{-1} \left( \begin{bmatrix} e_{refd} \\ e_{refq} \end{bmatrix} - \begin{bmatrix} e_d \\ e_q \end{bmatrix} \right) \\ &= \frac{1}{(Ls + R)^2 + (\omega L)^2} \begin{bmatrix} (Ls + R)\Delta u_d + \omega L\Delta u_q \\ (Ls + R)\Delta u_q - \omega L\Delta u_d \end{bmatrix} \end{aligned} \quad (9)$$

where  $e_{refd}$  and  $e_{refq}$  are d-axis and q-axis components of voltage command  $e_{ref}$ ;

$$\begin{bmatrix} \Delta u_d \\ \Delta u_q \end{bmatrix} = \begin{bmatrix} e_{refd} \\ e_{refq} \end{bmatrix} - \begin{bmatrix} e_d \\ e_q \end{bmatrix}$$

The positive and negative sequence separation control of grid voltage is adopted to ensure the three-phase current balance. The TOGI module is added before the positive and negative sequence separation module of grid voltage to eliminate the influence of the DC component. A modified DSC after the positive sequence current command is used to obtain a new current command and to eliminate the harmonic component in the current command. The calculation block diagram of the improved positive sequence current command is shown in Fig. 3.

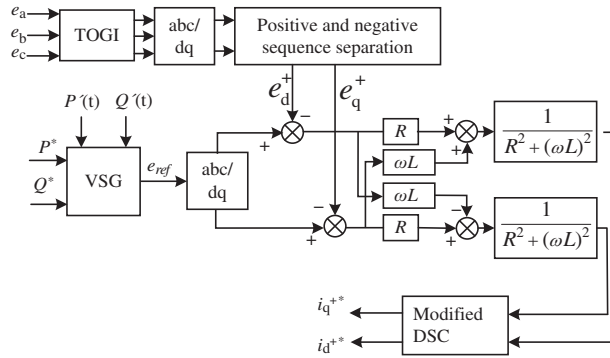


**Figure 3:** Improved calculation block diagram of positive sequence current command

### 4.2 Elimination of DC Component by Third-Order Generalized Integrator

Assume that the input signal is

$$u(t) = A_0 + A_1 \sin(\omega_0 t + \varphi) \tag{10}$$

Then the output of the third-order generalized integrator (TOGI) is

$$\begin{bmatrix} u_{1\infty}(t) \\ u_{2\infty}(t) \\ u_{3\infty}(t) \end{bmatrix} = \begin{bmatrix} 0 \\ kA_0 \\ kA_0 \end{bmatrix} + \begin{bmatrix} A_1 \sin(\omega_0 t + \varphi) \\ -A_1 \cos(\omega_0 t + \varphi) \\ 0 \end{bmatrix} \tag{11}$$

It can be seen from (11) that the DC bias component in  $u_{1\infty}(t)$  is eliminated, and the amplitude and phase are consistent with the AC quantity of the input signal. Thus, the influence of the DC component on the current command calculation can be eliminated according to TOGI. The structure of TOGI is shown in Fig. 4.

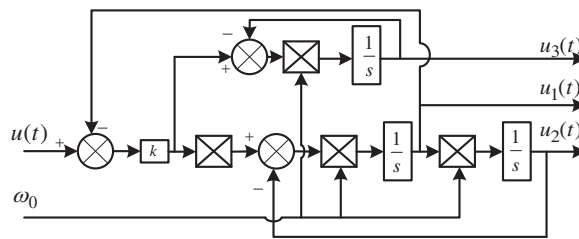


**Figure 4:** TOGI structure block diagram

### 4.3 Modified DSC

The transfer function of traditional DSC in s domain is

$$DSC_n(s) = \frac{1 + e^{j2\pi/n} e^{-(T/n)s}}{n} \tag{12}$$

where  $n$  is the delay coefficient, and  $T$  is the fundamental period of the grid.

To eliminate harmonics, traditional DSC usually consists of multiple  $DSC_n$  in series [24], and only odd harmonics can be filtered. In this paper, it is necessary to eliminate Even harmonics in the dq coordinate system should be eliminated, to improve traditional DSC. The modified DSC (MDSC) function expression is as follows:

$$MDSC(s) = \frac{1 + e^{j2\pi/n_s} e^{-(T/n)s}}{n} \tag{13}$$

The modified DSC function has  $n_s$  and  $n$  variables, which can better design the required frequency characteristics. In this paper,  $n = 4$  and  $n_s = 1$  are used. The function expression of MDSC is

$$MDSC(s) = \frac{1 + e^{-(T/4)s}}{n} \tag{14}$$

Its implementation in the time domain can be simplified as shown in Fig. 5.

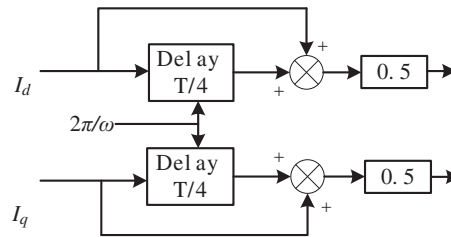


**Figure 5:** Time domain implementation block diagram of MDSC

The Bode diagram of MDSC is shown in Fig. 6.

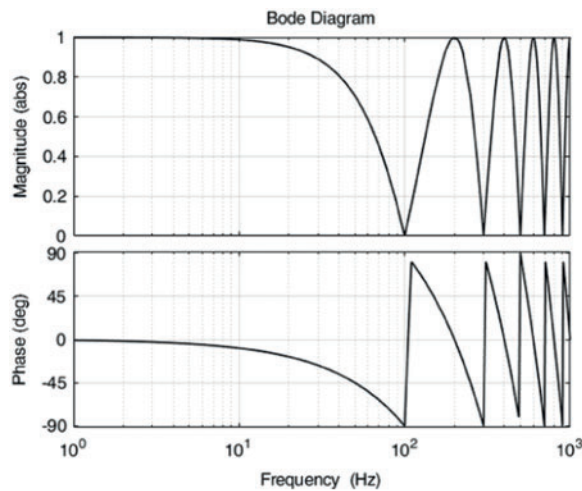


**Figure 6:** Bode diagram of MDSC

It can be seen from Fig. 6 that the modified DSC can completely filter even harmonics such as 100, 300 and 500 Hz.

#### 4.4 Calculation of Current Negative Sequence Instruction

##### 4.4.1 Control the Balance of Three-Phase Current

In order to make the output current follow the current reference value mentioned above, the output current of VSG will keep balance. At this time, the negative sequence current instructions  $i_d^{+*}$  and  $i_q^{+*}$  are all zero.

##### 4.4.2 Control the Active Power Constant

When the active power must be constant, it can be seen from Eq. (3). The amplitudes of active power fluctuation components  $P_{s2}$  and  $P_{c2}$  need to be zero

$$\begin{bmatrix} u_q^- & -u_d^- \\ u_d^- & u_q^- \end{bmatrix} \begin{bmatrix} i_d^{+*} \\ i_q^{+*} \end{bmatrix} + \begin{bmatrix} -u_q^+ & u_d^+ \\ u_d^+ & u_q^+ \end{bmatrix} \begin{bmatrix} i_d^{-*} \\ i_q^{-*} \end{bmatrix} = 0 \quad (15)$$

Then when the active power is constant, the negative sequence current command can be obtained from Eq. (15)

$$\begin{bmatrix} i_d^{-*} \\ i_q^{-*} \end{bmatrix} = -\frac{1}{(u_d^+)^2 + (u_q^+)^2} \begin{bmatrix} -u_q^+ u_q^- + u_d^+ u_d^- & u_q^+ u_d^- + u_d^+ u_q^- \\ u_d^+ u_q^- + u_q^+ u_d^- & u_q^+ u_q^- - u_d^+ u_d^- \end{bmatrix} \begin{bmatrix} i_d^{+*} \\ i_q^{+*} \end{bmatrix} \quad (16)$$

##### 4.4.3 Control the Constant Reactive Power

When the reactive power must be constant, the amplitudes of the reactive power fluctuation components  $Q_{s2}$  and  $Q_{c2}$  need to be zero

$$\begin{bmatrix} u_q^- & -u_d^- \\ u_d^- & u_q^- \end{bmatrix} \begin{bmatrix} i_d^{+*} \\ i_q^{+*} \end{bmatrix} - \begin{bmatrix} -u_q^+ & u_d^+ \\ u_d^+ & u_q^+ \end{bmatrix} \begin{bmatrix} i_d^{-*} \\ i_q^{-*} \end{bmatrix} = 0 \quad (17)$$

When the reactive power is constant, the negative sequence current command can be obtained from Eq. (17)

$$\begin{bmatrix} i_d^{-*} \\ i_q^{-*} \end{bmatrix} = \frac{1}{(u_d^+)^2 + (u_q^+)^2} \begin{bmatrix} -u_q^+ u_q^- + u_d^+ u_d^- & u_q^+ u_d^- + u_d^+ u_q^- \\ u_d^+ u_q^- + u_q^+ u_d^- & u_q^+ u_q^- - u_d^+ u_d^- \end{bmatrix} \begin{bmatrix} i_d^{+*} \\ i_q^{+*} \end{bmatrix} \quad (18)$$

#### 4.5 Current Inner Loop Improved QPR Cascade PI Control

The ideal proportional resonance (PR) regulator has infinite gain at the resonance frequency, and can realize the static error-free tracking of AC signal, but it has a certain influence on the system's stability. Therefore, this paper adopts the QPR regulator. The transfer function of QPR is as follows

$$G_{QPR}(s) = k_{QPR} + \frac{2k_r \omega_c s}{s^2 + 2\omega_c s + \omega_0^2} \quad (19)$$

where  $k_{QPR}$  is the proportional coefficient and  $k_r$  is the integral time coefficient;  $\omega_0$  represents the resonant frequency;  $\omega_c$  is the cut-off frequency.

QPR at resonant frequency  $\omega_0$  The gain is

$$|G_{QPR}(j \pm \omega_0)| = k_{QPR} + k_r \quad (20)$$

It can be seen from Eq. (20) that for the frequency of  $\pm\omega_0$  The gain of  $k_{QPR} + k_r$  can be obtained by the QPR regulator.

For AC input, at resonant frequency  $\omega_0$  When only PI regulator is used in the current controller, the gain is

$$|G_{PI}(j\omega_0)| = \sqrt{k_p^2 + \left(\frac{k_i}{\omega_0}\right)^2} \tag{21}$$

This paper adopts the improved QPR cascade PI control strategy with harmonic control to eliminate the 5th, 7th, 11th, and 13th harmonics in a three-phase static coordinate system, that is, the 6th and 12th harmonics in the dq coordinate system. The structure block diagram is shown in Fig. 7.

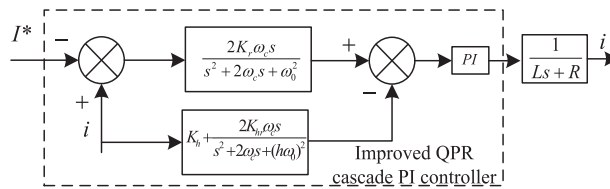


Figure 7: Improved QPR cascade PI control block diagram

The proportional term of the fundamental control part QPR is removed to reduce the gain of the non-resonant point,. According to Fig. 7, the transfer function of the reference current to the output current is expressed as

$$G(s) = \frac{i(s)}{I^*(s)} = \frac{G_{QPR1} G_{PI} G_{sys}}{1 + G_{PI} G_{sys} (G_{QPR1} + G_{QPR6} + G_{QPR12})} \tag{22}$$

where:

$$G_{QPR1} = \frac{2k_r\omega_c s}{s^2 + 2\omega_c s + \omega_0^2}, \quad G_{QPR6} = k_6 + \frac{2k_{6r}\omega_c s}{s^2 + 2\omega_c s + (6\omega_0)^2}, \quad G_{QPR6} = k_6 + \frac{2k_{6r}\omega_c s}{s^2 + 2\omega_c s + (6\omega_0)^2},$$

$$G_{sys} = \frac{1}{Ls + R}$$

The bode diagram corresponding to Eq. (22) is shown in Fig. 8.

Fig. 8 shows that the closed-loop transfer function of reference current to output current gains 1 at 50 Hz of the base wave current, zero phase response, low gain outside the resonance point, and zero gain at the 6th and 12th harmonic. It can be seen that the improved QPR cascade PI control strategy can track the fundamental current in the reference instruction without static difference and effectively suppress the harmonic current. The improved positive sequence current inner loop controller block diagram is shown in Fig. 9.

Similarly, the negative sequence current inner loop control block diagram is consistent with the positive sequence current inner loop control block diagram, and the control quantity is the negative sequence component.

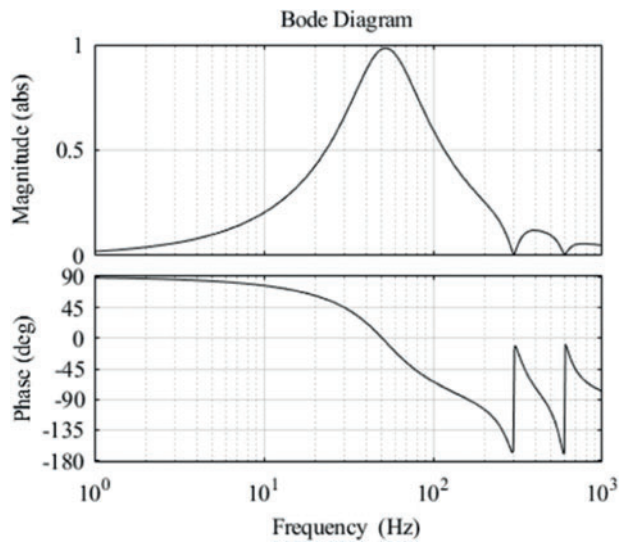


Figure 8: Bode diagram of improved QPR cascade PI

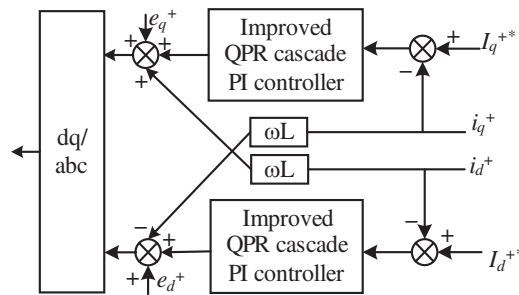


Figure 9: Improved positive sequence current inner loop controller block diagram

### 5 Simulation Analysis

The simulation results show that the traditional current control strategy and the improved balanced current control strategy proposed in this paper are simulated by Matlab/Simulink software. The simulation parameters are as follows (Table 1).

First, the balance current control is taken as the goal. The simulation duration is 2 s. The grid voltage is normal within 0~0.5 s, the voltage amplitude of phase A drops to 240 V within 0.5~1 s, and the grid voltage contains 5 times, 7 times, and 11 times. Sub-harmonics within 1~1.5 s, the power grid A phase contains 15 V DC component within 1.5~2 s.

Fig. 10 shows the three-phase current waveform under common VSG control balanced current under unbalanced voltage.

It can be seen from Fig. 10 that common VSG control balanced current under unbalanced voltage when the power grid is normal. The current can achieve a three-phase balance with a current amplitude of 32.4 A.

When the A-phase voltage amplitude drops to 240 V, the common VSG control balanced current under unbalanced voltage can still maintain the current balance, and the current amplitude is 34.3 A.

**Table 1:** Parameters of the simulation model

Parameter name	Value and unit	Parameter name	Value and unit
DC power supply $U_{dc}$	800 V	Inverter side resistance $R_s$	0.1 $\Omega$
Effective value of AC phase voltage	220 V	Grid side resistance $R_g$	0.1 $\Omega$
Inverter side inductance $L_s$	5 mH	Filter capacitor C	20 $\mu$ F
Grid side inductance $L_g$	3 mH	$k_r$	100
$k_{6r}$	200	$k_{12r}$	250
$k_6$	1	$K_{12}$	1
Given value of active power $p^*$	15 Kw	Reactive power set value $Q^*$	0 Kvar

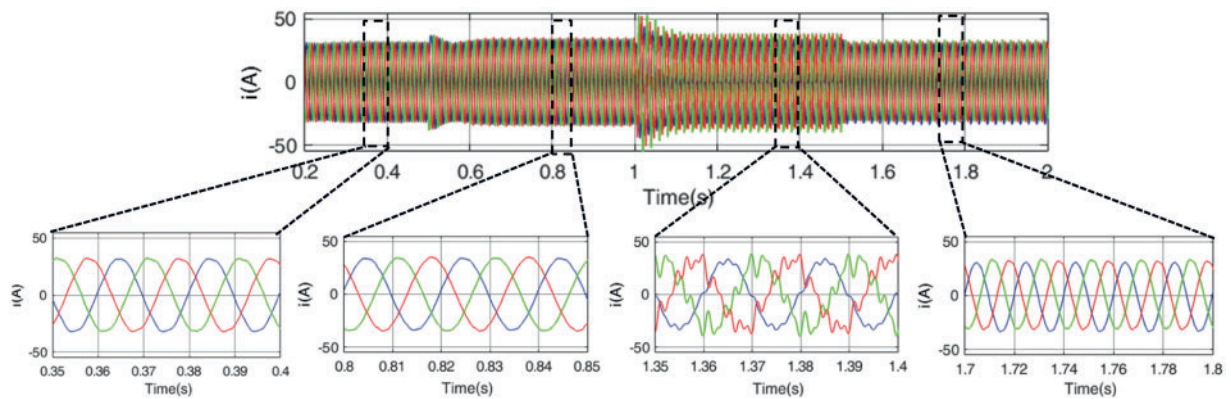


**Figure 10:** Common VSG control balanced current under unbalanced voltage

When the grid voltage contains harmonics, the output current of common VSG control balanced current under unbalanced voltage will contain harmonics. The harmonic distribution of the three-phase current is shown in Fig. 11, and the harmonic distribution of the phase A, phase B, and phase C is from left to right.

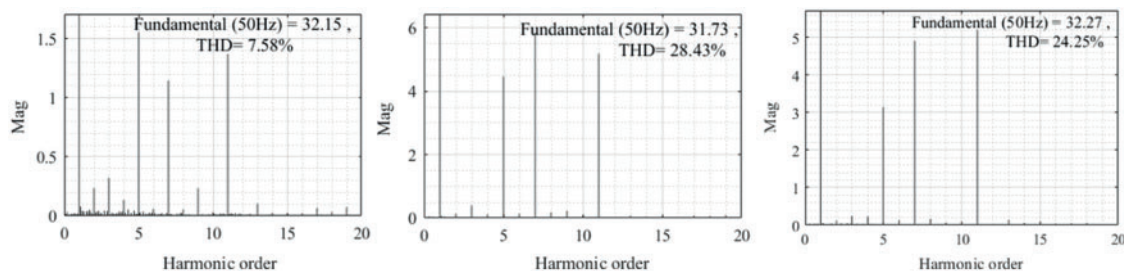


**Figure 11:** Harmonic distribution of three-phase current controlled by common VSG in power grid with harmonics

It can be seen from Fig. 11 that the harmonic content of common VSG control balanced current under unbalanced voltage-controlled three-phase current exceeds the allowable range of grid connection, and the voltage harmonic of phase B reaches 28.43%.

When the grid voltage contains a small amount of DC component, it can be seen from Fig. 10 that the three-phase current will be unbalanced, and the degree of imbalance is 23.3%, which seriously affects the power quality.

Under the same simulation conditions, the output three-phase current waveform of the proposed VSG control strategy under complex conditions is shown in Fig. 12.

It can be seen from Fig. 12 that the VSG control strategy under complex conditions can well control the three-phase balance of output current when the grid voltage is normal, unbalanced, with harmonic and DC components. When the grid voltage contains DC components, the unbalance degree is 1.4%, which is 93.9% lower than the VSG control strategy under ordinary unbalanced voltage.

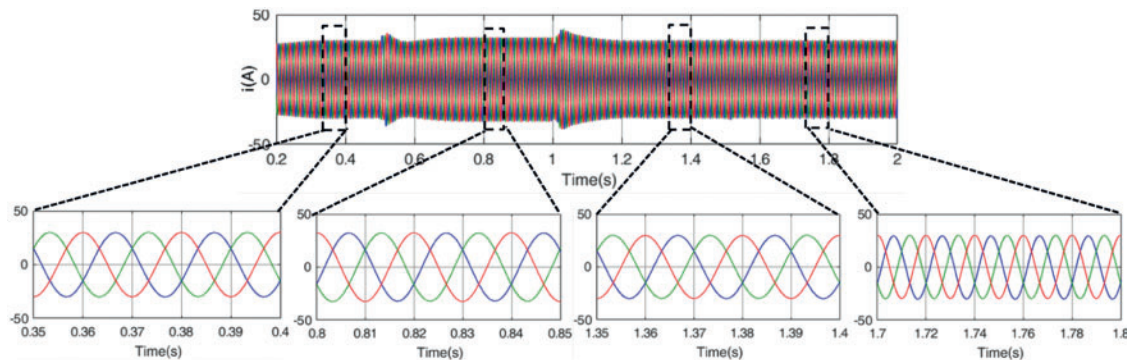


**Figure 12:** VSG control balance current under complex grid conditions

The harmonic distribution of VSG control strategy under complex conditions is shown in Fig. 13, and the harmonic distribution of phase A, phase B and phase C is in turn from left to right.

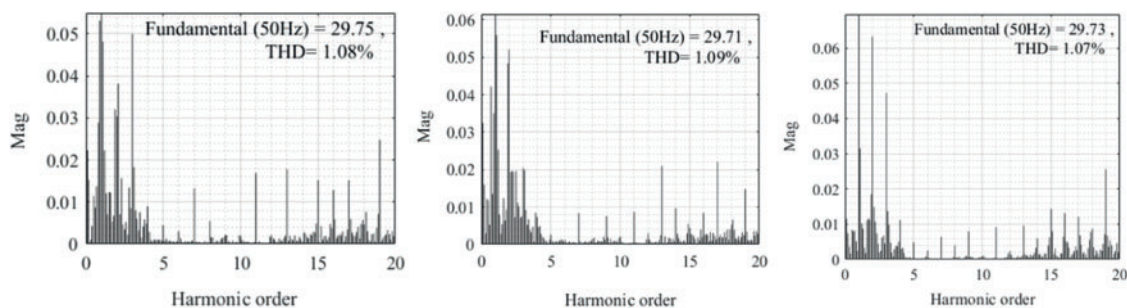


**Figure 13:** Harmonic distribution of VSG control current under complex conditions with harmonics in the power grid

According to the harmonic distribution diagram 13, the output current harmonics can be completely suppressed by the VSG control strategy under complex conditions when the grid voltage has harmonics. The current THD of phase A, phase B, and phase C is reduced from 7.58% to 1.08%, 28.43% to 1.09%, and 24.25% to 1.07%, respectively. The harmonic content is greatly reduced to meet the requirements of the grid-connected harmonic content standard.

Under the current balance control target, the power waveforms of the traditional balance current control strategy and the comprehensive control strategy under complex conditions are shown in Fig. 14.

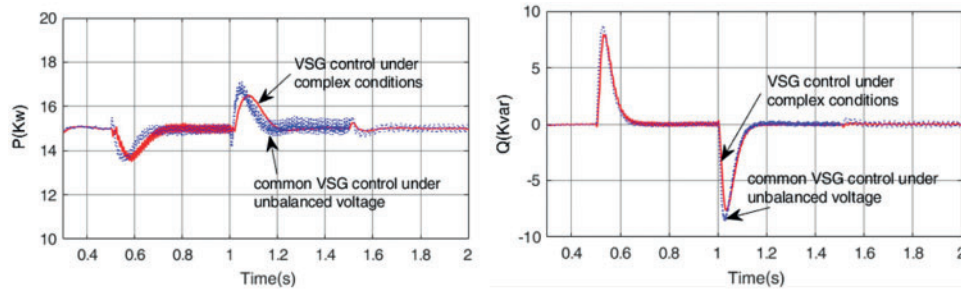


**Figure 14:** Power waveform under current balance control target

It can be seen from Fig. 14 that under normal grid voltage and three-phase unbalanced conditions, the power control of traditional common VSG control balanced current under unbalanced voltage and VSG control strategy under complex conditions are the same. However, when there are harmonics and DC components, the power of traditional VSG control under unbalanced voltage fluctuates. In contrast, VSG control under complex conditions can control constant power.

Under the same simulation conditions as the current balance control objective, the proposed scheme is verified with the a constant active power control objective.

Fig. 15 shows the current, active, and reactive power waveforms controlled by VSG under constant active power and complex working conditions.

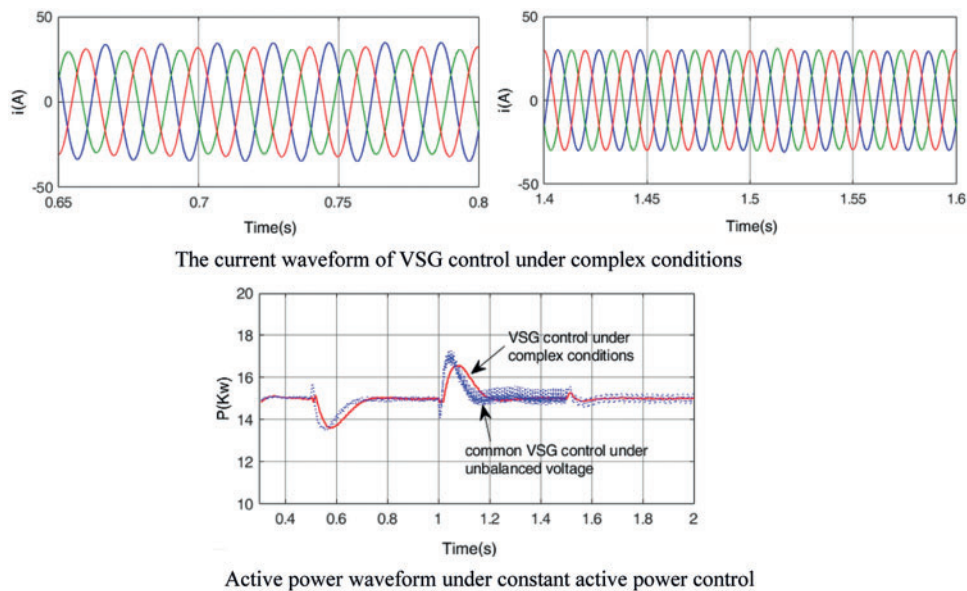


**Figure 15:** VSG control under complex conditions with constant active power

According to Fig. 15, under the active power constant control target, when the grid voltage is unbalanced, the three-phase current will be unbalanced as that of common VSG control balanced

current under unbalanced voltage. However, for the grid voltage containing harmonic and micro-DC components, the proposed strategy can establish that the output current meets the grid connection requirements and the active power is constant. But the active power still fluctuates under common VSG control balanced current under unbalanced voltage.

Under the target of constant reactive power, the reactive power waveforms under the two control strategies are shown in Fig. 16.

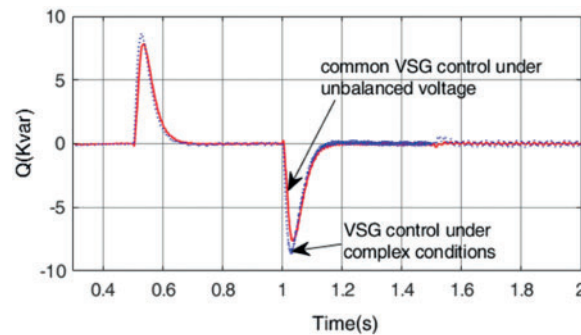


**Figure 16:** Power waveform under constant reactive power control target

It can be seen from Fig. 16 that under the target of constant reactive power and, the common VSG control under unbalanced voltage has fluctuation in reactive power when the grid voltage contains harmonic and trace DC content.

## 6 Conclusion

In this paper, VSG control strategy is proposed in the complex condition to realize grid-connected current to meet the grid connection requirements under complex voltage conditions, in the case of unbalanced three-phase voltage, harmonic and small DC components. The harmonic current is controlled by using TOGI to eliminate DC components, improve DSC and QPR cascade pi to control harmonic current. The harmonic content and unbalance degree meet the grid connection standard when grid-connected current balance is used for control purposes under the non-ideal grid voltage. Compared with the common VSG control balanced current under unbalanced voltage, VSG control under complex conditions can be applied in the multi-operation condition of power grid voltage. Finally, the control strategy can still achieve the control target under the condition that the power is constant for the control purpose.

**Funding Statement:** This work was funded by the National Natural Science Foundation of China (61863023).

**Conflicts of Interest:** The authors declare that they have no conflicts of interest to report regarding the present study.

## References

1. Qi, W., Li, Y., Fang, F., Ding, L. (2019). Research on VSG grid-controlled strategy based on energy-stored quasi-Z-source inverter. *Power System Protection and Control*, 47(4), 124–133. DOI 10.7667/PSPC180337.
2. Bevrani, H., Ise, T., Miura, Y. (2014). Virtual synchronous generators: A survey and new perspectives. *International Journal of Electrical Power & Energy Systems*, 54, 244–254. DOI 10.1016/j.ijepes.2013.07.009.

3. Shi, K., Ye, H., Song, W., Zhou, G. (2018). Virtual inertia control strategy in microgrid based on virtual synchronous generator technology. *IEEE Access*, 6, 27949–27957. DOI 10.1109/ACCESS.2018.2839737.
4. Zhang, J., Wang, N., Huang, R., Ma, M., He, S. (2019). Survey on frequency regulation technology of power grid by high-penetration photovoltaic. *Power System Protection and Control*, 47(15), 179–186. DOI 10.19783/j.cnki.pspc.181042.
5. Zhang, F., Piao, Z., Guo, Y., Zhang, X., Zhou, J. (2020). Research on adaptive control VSG rotation inertia. *Acta Energiæ Solaris Sinica*, 41(10), 93–100.
6. Liu, J., Yang, D., Yao, W., Fang, R., Zhao, H. et al. (2017). PV-Based virtual synchronous generator with variable inertia to enhance power system transient stability utilizing the energy storage system. *Protection and Control of Modern Power Systems*, 2(1), 1–8. DOI 10.1186/s41601-017-0070-0.
7. Yang, Y., Mei, F., Zhang, C., Miao, H., Chen, H. et al. (2019). Coordinated adaptive control strategy of rotational inertia and damping coefficient for virtual synchronous generator. *Electric Power Automation Equipment*, 39(3), 125–131. DOI 10.16081/j.issn.1006-6047.2019.03.020.
8. Wu, H., Ruan, X., Yang, D., Chen, X., Zhong, Q. et al. (2015). Modeling of the power loop and parameter design of virtual synchronous generators. *Proceedings of the CSEE*, 35(24), 6508–6518. DOI 10.13334/j.0258-8013.pcsee.2015.24.027.
9. Liu, J., Miura, Y., Ise, T. (2016). Comparison of dynamic characteristics between virtual synchronous generator and droop control in inverter-based distributed generators. *IEEE Transactions on Power Electronics*, 31(5), 3600–3611. DOI 10.1109/TPEL.2015.2465852.
10. Cheema, K. M., Milyani, A. H., El-Sherbeeny, M. A., El-Meligy, M. A. (2021). Modification in active power-frequency loop of virtual synchronous generator to improve the transient stability. *International Journal of Electrical Power & Energy Systems*, 128, 106668. DOI 10.1016/j.ijepes.2020.106668.
11. Cheema, K. M., Mahmood, R. S., Tahir, M. F., Mehmood, K., Javed, M. Y. et al. (2021). Modified control of virtual synchronous generator for microgrid stability improvement. *2021 International Bhurban Conference on Applied Sciences and Technologies (IBCAST)*. DOI 10.1109/IBCAST51254.2021.9393174.
12. Geng, Y., Tian, F., Sun, S., Wei, C., Zhang, Y. (2018). A method of current harmonics suppression based on VSG. *Transactions of China Electrotechnical Society*, 33(5), 1040–1050. DOI 10.19595/j.cnki.1000-6753.tces.170093.
13. Alipoor, J., Miura, Y., Ise, T. (2014). Voltage sag ride-through performance of virtual synchronous generator. *Power Electronics Conference*, pp. 3298–3305. Hiroshima, Japan. DOI 10.1109/IPEC.2014.6870160.
14. Li, Z., Zhang, Z., Liu, H., Song, P., He, T. et al. (2020). Harmonic resonance characteristics analysis and suppression strategy of LCL energy storage virtual synchronous generator. *Acta Energiæ Solaris Sinica*, 41(10), 101–108.
15. Wan, X., Hu, H., Nie, X., Yu, Y., Zeng, F. (2017). An improved control strategy for virtual synchronous generator under unbalanced grid voltage. *Power System Technology*, 41(11), 3573–3581. DOI 10.13335/j.1000-3673.pst.2016.3212.
16. Yang, M., Gao, L., Wang, H., Du, S., Li, B. (2019). Coordinate control of power and current for virtual synchronous generator under unbalanced grid voltage. *Power System Protection and Control*, 47(6), 17–23. DOI 10.7667/PSPC180392.
17. Hu, H., Wan, X., Ding, X., Yu, Y. (2020). Improved low voltage ride-through control strategy for distributed virtual synchronous generator. *Electric Machines and Control*, 24(1), 145–155. DOI 10.15938/j.emc.2020.01.018.
18. Luo, D., Chen, Z., Huang, S., Guo, D. (2013). A novel field-weakening control strategy for interior permanent magnet synchronous motor. *Journal of Human University (Natural Sciences)*, 40(3), 59–64. DOI 10.3969/j.issn.1674-2974.2013.03.011.
19. Xiao, X., Chen, M. (2017). Power control of virtual synchronous generator under unbalanced grid voltage. *Electric Power Automation Equipment*, 37(8), 193–200. DOI 10.16081/j.issn.1006-6047.2017.08.026.

20. Xie, J., Xie, Z., Lin, M. (2020). Control strategy of current balance based on VSG of DFIG under unbalanced grid voltage conditions. *39th Chinese Control Conference*, pp. 5293–5298. Shenyang, China. DOI 10.23919/CCC50068.2020.9189131.
21. Shi, K., Song, W., Xu, O., Liu, R., Fang, Z. et al. (2017). Low-voltage ride-through control strategy for a virtual synchronous generator based on smooth switching. *IEEE Access*, 6, 2703–2711. DOI 10.1109/ACCESS.2017.2784846.
22. Chen, T., Chen, L., Wang, Y., Zheng, Y., Mei, S. (2016). Balanced current control of virtual synchronous generator considering unbalanced grid voltage. *Power System Technology*, 40(3), 904–909. DOI 10.13335/j.1000-3673.pst.2016.03.035.
23. Feng, W., Sun, K., Guan, Y., Guerrero, J., Xiao, X. (2018). An active harmonic grid-connecting current suppression strategy for hierarchical control based microgrid. *Transactions of China Electrotechnical Society*, 33(6), 1400–1409. DOI 10.19595/j.cnki.1000-6753.tces.170691.
24. Hui, N., Wang, D., Li, Y. (2018). DC-Offset elimination method for grid-connected phase-Locked Loop by modified DSC. *Journal of Northeastern University (Natural Science)*, 39(11), 1526–1531. DOI 10.12068/j.issn.1005-3026.2018.11.002.